Archives of Acoustics Vol. 50, No. 4, pp. 513–524 (2025), https://doi.org/10.24425/aoa.2025.156934

OSA 2025

Potential Applications of Ultrasonic Parametric Array Loudspeakers (PALs) in Room Acoustic Measurements

Filip WĘGRZYN*, Adam PILCH

AGH University of Krakow
Kraków, Poland

*Corresponding Author e-mail: filipwegrzyn@agh.edu.pl

Received September 8, 2025; revised November 5, 2025; accepted November 12, 2025; published online November 20, 2025.

In this paper, the potential use of parametric array loudspeakers (PALs) in acoustic measurements of the room is analysed, especially in the assessment of the effectiveness of reflective panels and intentionally angled surfaces. PALs are sound sources capable of emitting highly directional acoustic beams within the audible frequency range. Their operation is based on the emission of a high-frequency (ultrasonic) carrier modulated so that, through nonlinear demodulation in air, audible sound is generated. This process results in a narrow, focused sound beam, enabling precise acoustic emission. To explore PALs potential for acoustic measurement applications, the propagation behaviour of PAL-generated signals is first investigated under free-field conditions, focusing on how different surface types influence sound reflection. Subsequent experiments are carried out in a controlled indoor space, where impulse responses are recorded for various beam incidence angles and receiver positions. The collected data are used to generate sound-level distribution maps, allowing for the visualization and quantification of reflected sound coverage areas. The results show that PALs produce beams with substantially reduced lateral dispersion compared to conventional loudspeakers, enabling precise identification of reflection points and incidence angles. This directional precision makes it possible to accurately assess how effectively the reflective acoustic elements and structures shape the sound field within the room. Overall, these findings may contribute to optimising sound design in acoustically complex environments.

Keywords: parametric array loudspeakers (PALs); room acoustics; ultrasonic; reflection; directivity.

1. Introduction

Localising acoustic flaws in rooms is one of the key problems in modern acoustics. Most measurements use omnidirectional speakers to record the room's impulse response, which can later be processed and analysed. However, the omnidirectionality of such a speaker causes the measurement to include reflections from every element in the room. As a result, the influence of certain elements may be masked in the recording (Gallien *et al.*, 2024). Using a speaker with high directivity may allow the user to examine only a chosen structure, such as a reflective panel or a diffusor. Additionally, high directivity enables easier tracking of the first reflection, which is, if not properly managed, one of the most common causes of acoustic flaws in rooms.

In order to obtain a sufficiently narrow beam that can generate sound waves in one direction only, some speakers utilise the parametric array effect. This effect was discovered in the early 1960s by Westervelt (1963). He demonstrated that, in theory, an end-fire array of virtual sources at the difference frequency can be produced by the interaction of two intense, collimated beams with slightly different high frequencies. These virtual sources arise because the instantaneous sound speed, which is one of the physical parameters depends inherently on the sound pressure or particle velocity. The resulting virtual end-fire array generated by this nonlinear interaction is therefore referred to as a parametric acoustic array, or simply a parametric array (Gan *et al.*, 2012a). When two primary waves of frequencies f_1 and f_2 ($f_2 > f_1$) are fully confined

beams, the angle at which the sound intensity of the difference frequency $f = f_2 - f_1$ is reduced by one-half (3 dB), is approximately given by

$$\theta_h \approx \sqrt{2\alpha_T/k}, \tag{1}$$

where k is the wavenumber of the difference-frequency wave, and α_T is the total sound absorption coefficient of the primary waves (Gan *et al.*, 2012b).

Amplitude modulation of ultrasonic carrier waves was introduced by Berktay (1965), who managed to substitute the tonal difference-frequency with a full frequency spectrum. Later, after Bennett and Blackstock (1975) successfully carried out the parametric array experiment in air (Gan *et al.*, 2012b), the phenomenon was utilised in audio applications by Yoneyama *et al.* (1983). When used as a parametric array loudspeaker (PAL), audible sound can be generated through the self-demodulation of the carrier's ultrasound and with the high directivity inherited from the parametric array (Ju, Kim, 2010).

Previous research in the field of room acoustics employed high-directivity speakers for tracing reflection paths or obtaining spatial impulse responses (Tervo *et al.*, 2009). However, while multiple studies analyse reflective elements mostly under laboratory conditions, in-situ measurements usually focus on tracing reflection paths in general, without assessing the performance of a singular reflector or diffusor. This paper studies potential applications of said speakers, focusing on the analysis of modulated sound reflections generated by PALs from different surfaces of varying sizes and materials.

The aim of this study is to determine whether the PALs can serve as a tool for identifying sources of acoustic flaws in rooms, such as determining the effectiveness of reflective panels or intentionally angled surfaces.

2. Laboratory measurements

All measurements were performed using a Videotel Digital HyperSound HSS 3000 speaker (Videotel Digital, 2014). First, the frequency response and directivity index were measured using a Klippel GmbH near-field scanner (NFS). The NFS performs holographic measurements of the near-field sound pressure to obtain a set of coefficients that precisely characterise the sound pressure at any point within the three-dimensional field outside the scanning surface. By leveraging the benefits of near-field measurements and applying spherical harmonic wave expansion, the near-field data can be extrapolated into the far field. This expansion enables high spatial resolution with fewer measurement points, and the post-processed results are both faster to obtain and more comprehensive than those from conventional directivity-measurement techniques (Login, 2015). The Klippel setup with the PAL mounted is shown in Fig. 1.

Fig. 1. Klippel GmbH near-field scanner measurement setup.

Secondly, the directivity of the sound reflected from different surfaces was measured in an anechoic chamber. The test surfaces included three plates: a wooden plate (140 cm × 140 cm), a wooden plate (40 cm × 40 cm), and an acrylic glass plate (40 cm × 40 cm). To test directivity, the PAL was placed at a 45° angle, 2.5 m from the plate placed in the middle of the chamber. The microphone was positioned on a crane-style arm on the opposite side of the chamber, oriented to record sound reflected from the plate at the chosen angle. The distance between the plate and the microphone was also equal to 2.5 m. In this setup, the crane-style arm was automatically repositioned after each measurement, maintaining the same distance while simultaneously adjusting the angle. Consequently, a directivity pattern of the reflected sound was achieved, with a resolution of 2° over the range of 15°–75°. A wider range was not necessary as signal levels outside this interval reached the noise floor values. The complete setup is shown in Fig. 2. All sounds were recorded using a GRAS 46AE 1/2″ CCP free-field standard microphone.

Fig. 2. Directivity of reflected sound, measurement setup in an anechoic chamber.

3. Results of laboratory measurements

For comprehensiveness, the obtained results are subdivided into two distinct segments. The initial seg-

ment shows speaker parameters acquired from the Klippel measurements, regarding the PAL's beamwidth and directivity, while the second segment presents polar plots of the reflected sound, generated from measurements performed in the anechoic chamber.

3.1. Directivity of a speaker

The Klippel NFS measurement was performed with a 5° resolution in a full 360° sphere around the speaker, with a frequency resolution of six points per octave. The frequency range was limited to 300 Hz–8000 Hz to shorten measurement time and match the frequency range of this PAL model, which starts at 300 Hz (Videotel Digital, 2014). Figure 3 shows the acquired directivity index (DI).

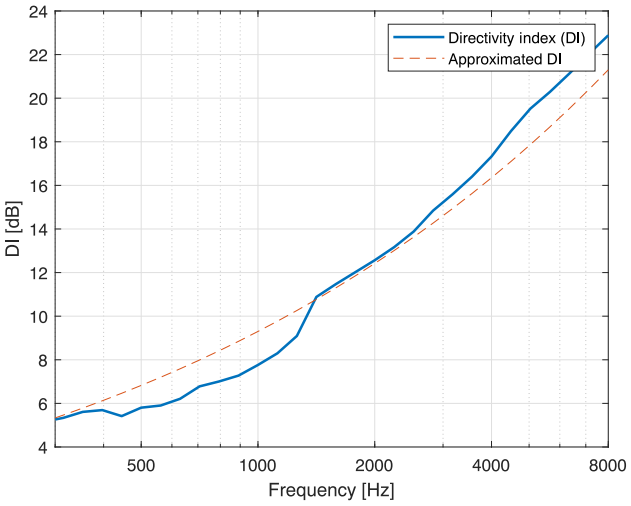

Fig. 3. Directivity index of the PAL (blue line) and approximated DI (red, dashed line).

The directivity index of the loudspeaker (Fig. 3) starts at around 5 dB at 300 Hz, then it reaches 10 dB at 1.5 kHz, and finally goes up to 23 dB at 8 kHz. The measured values were approximated with the function $12f^{1/3} - 2.7$, where f is the frequency in Hz. This approximation was based on the value of root mean square (RMS) difference between the measured and approximated values, which resulted in the lowest RMS value of 1.08 for the function given above.

A perfect theoretical cardioid has a directivity index of 4.8 dB; therefore, a directivity index of around 10 dB or more indicates a significantly directional loudspeaker (Vuine, 2024). Consequently, the analysed speaker achieves a highly concentrated beam only above 1.5 kHz. To study the precise beamwidth, a corresponding plot showing the PAL's beamwidth is presented in Fig. 4.

As illustrated in Fig. 4, for frequencies between 500 Hz–1000 Hz, the sound beam generated by the PAL reaches its maximum width of approximately 70° at a −6 dB sound pressure level (SPL) decrease. This

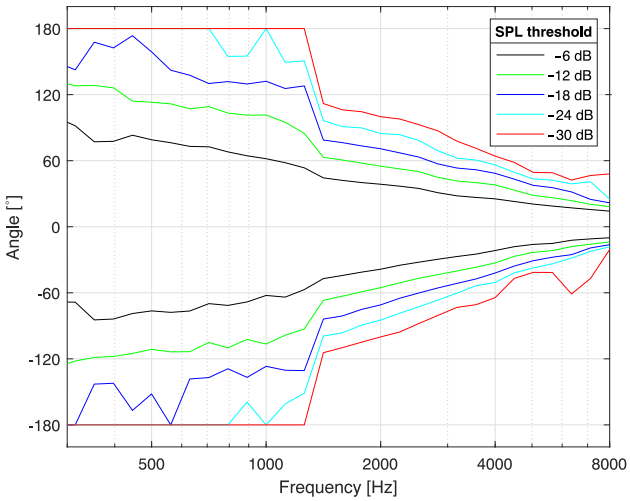

Fig. 4. Directivity (beamwidth) of the PAL.

threshold is usually taken as the beamwidth limit, since it is a value at which the signal power is halved (Keele, 2016). Afterwords, the beam slowly narrows, from 50° at 1.5 kHz to almost 20° at 5 kHz. Additionally, the SPL drop increases to −30 dB at just 40°. Sudden changes in beamwidth at lower SPL thresholds, visible around 1.5 kHz, are most likely caused by Klippel's internal algorithm switching to a different computation method.

3.2. Directivity of reflected sound

During the measurements in the anechoic chamber, directivity patterns of the reflected sound were obtained, each one for a different plate. The results are represented in the form of polar plots in Fig. 5, with six patterns corresponding to centre frequencies of octave bands ranging from 500 Hz to 16 kHz.

The widths of the reflected sound beam for a given frequency are summarised in Table 1. The limits for each beamwidth were assumed to be −6 dB on both sides, as in the Klippel measurement. In Fig. 5a, we can observe the directivity characteristic of the sound reflected from the large wooden plate. The strongest directivity is obtained at 16 kHz and 8 kHz. For the smaller wooden plate, the reflection pattern visible in Fig. 5b is nearly identical to the one obtained from the acrylic glass plate (Fig. 5c). Although the strongest directivity is also observed at the highest frequencies, at 500 Hz both the acrylic and small wooden plates have a reflected beamwidth of only 2°. This is most likely caused by the small size of the plates. Due to the larger area of the 140 cm × 140 cm wooden plate, the sound level measured in the 500 Hz bandwidth is substantially higher in comparison with two other plates. Additionally, there are no irregularities caused by an insufficient surface area size. Such irregularities would likely explain the unreasonably narrow angle observed for the small plates, since only a small

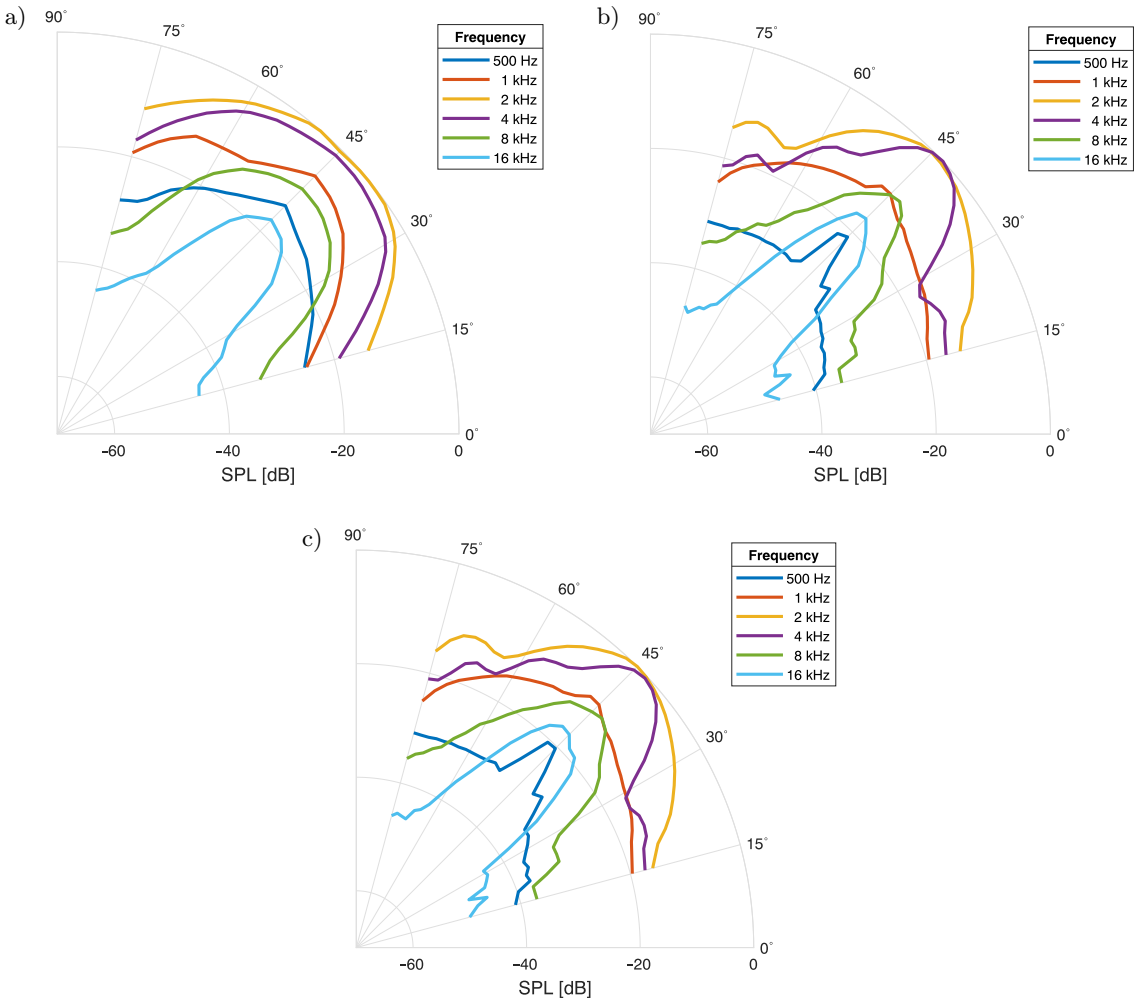

Fig. 5. Speaker angle −45°, polar plots of the PAL's directivity patterns reflected from: a) wooden plate (140 cm × 140 cm); b) wooden plate (40 cm × 40 cm); c) acrylic glass (40 cm × 40 cm).

Table 1. Width of the reflected beam for given frequencies and plate types.

Plate type	Reflected beamwidth angle					
	500 Hz	1 kHz	2 kHz	4 kHz	8 kHz	16 kHz
Wood – 140 cm × 140 cm	14°	14°	18°	18°	14°	10°
Wood – 40 cm × 40 cm	2°	18°	18°	10°	6°	6°
Acrylic – 40 cm × 40 cm	2°	18°	18°	10°	6°	6°

portion of the wave is reflected at the angle of incidence. It is apparent that the size of the sample affects the width of the reflected beam, which explains the substantial narrowing of the reflected angle compared to the beamwidth of the direct sound acquired with the Klippel system.

In summary, as long as the area of an analysed sample has a sufficiently large reflective area, there are no differences in the shapes of the polar patterns of the reflected sound. However, if the sample is too small, some frequencies will not be properly reflected, resulting in lower sound pressure levels and more irregular patterns. Furthermore, the obtained angles are significantly narrower than those acquired from the Klippel analysis. Larger sizes of the reflector result in a wider reflected sound beam.

4. Measurement of sound reflections from an angled ceiling

To verify the capabilities of parametric speakers in room acoustic analysis, a measurement of sound reflections from an angled ceiling was conducted. This measurement was performed in the WA3 classroom, inside the D1 building of AGH University of Krakow. The classroom has a part of ceiling angled at 5.25° to direct reflections from the lecturer to the students. The aim of the analysis was to determine whether the

angle of the ceiling is correct and whether the size of the plate is sufficient to distribute reflections from it evenly across the room.

To measure the sound reflected from the ceiling with a PAL, eight microphones were placed at random positions throughout the room. To avoid standing waves and reflections from the walls, all microphones were positioned off the main axis of the room and at least 1 m away from the walls. The height of each microphone was set to 1.2 m, which is the average height of a seated person (Rakerd, 2018). The parametric speaker was placed on a stand and angled so that the PAL aimed at the lower edge of the angled ceiling. The setup is visible in Fig. 6, while the theoretical model is shown in Fig. 7 (side view) and Fig. 8 (top view). For both source positions, five measurements of impulse responses were taken, each at a different PAL angle. The fifth measurement for position S1 was ignored due to obstruction from a projector in the path of the sound beam. A sine sweep from 300 Hz to 18 kHz was used as the excitation signal to match the bandwidth of this parametric speaker model (Videotel Digital, 2014).

Fig. 6. Experimental setup for measuring reflections from the angled ceiling in the classroom.

4.1. Results of measurements

From all recorded impulse responses, heatmaps of SPLs for each octave band were interpolated in the MATLAB programming environment. The maps are shown in Figs. 9–16. The horizontal line in each map marks the end of the angled ceiling. The interpolation area starts at the first row of desks. To limit the number of figures, results for the 8 kHz and 16 kHz bands were omitted, since these frequency bands are rarely used in room acoustic analysis.

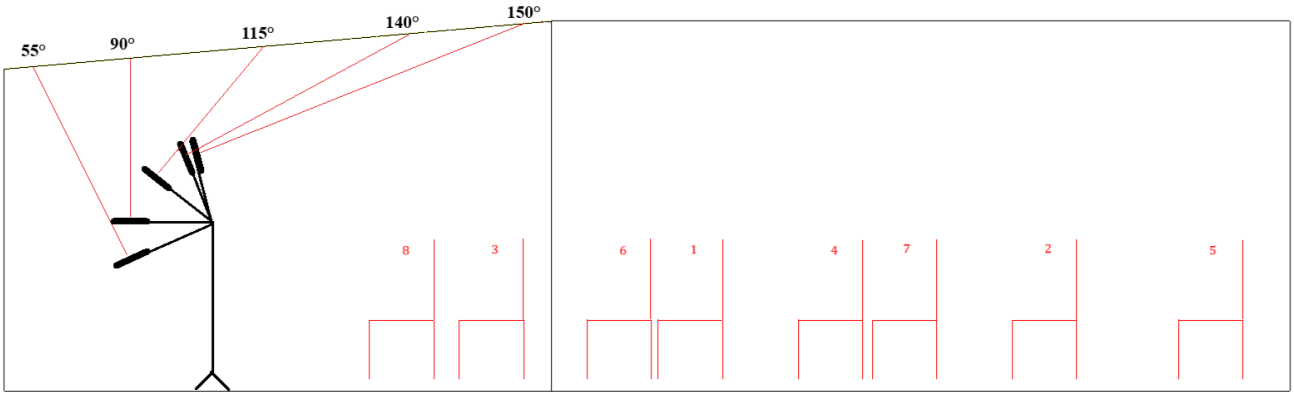

Fig. 7. Angled ceiling measurements, all microphone positions and speaker angles (side view).

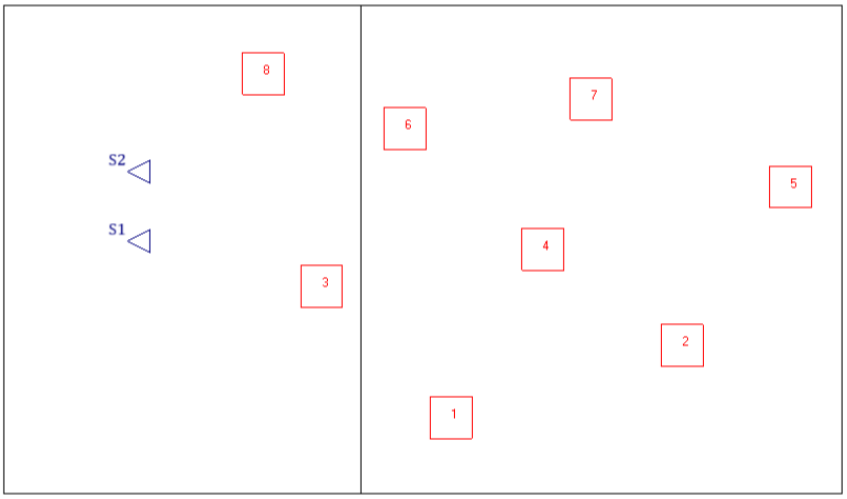

Fig. 8. Angled ceiling measurement, all microphone and speaker positions (top view).

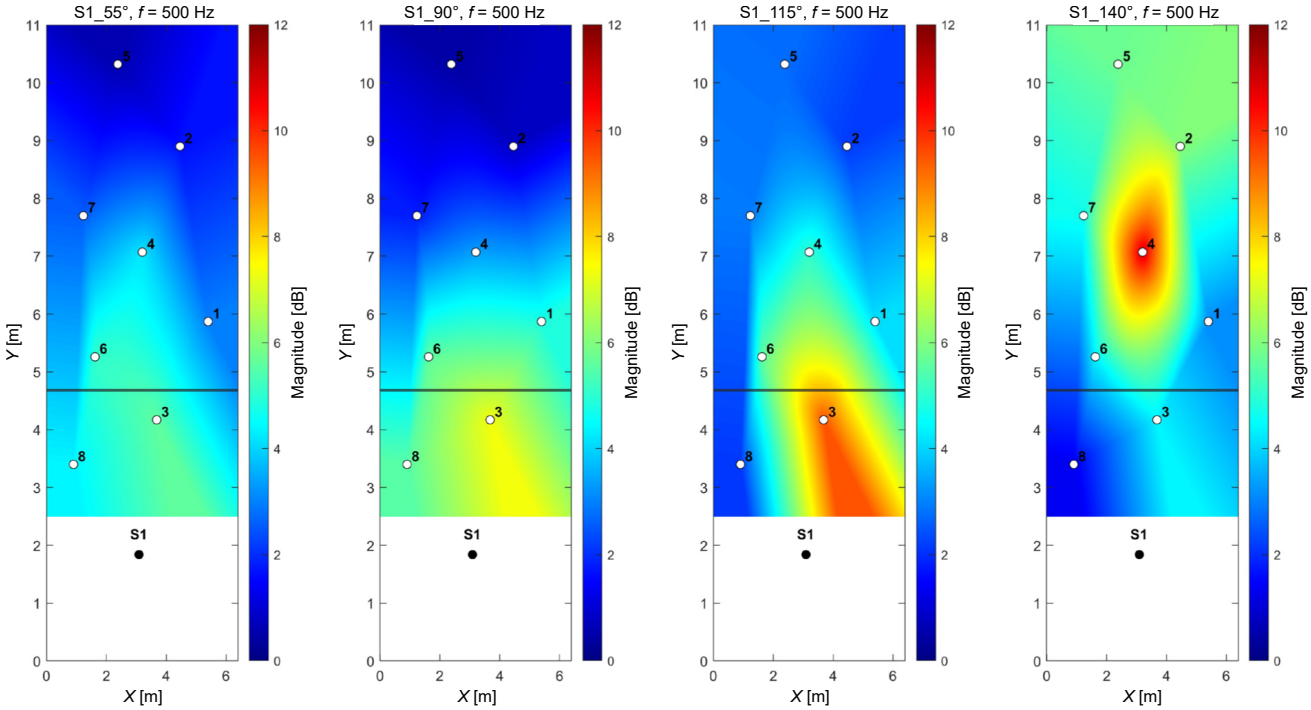

Fig. 9. SPL heatmaps for all PAL angles, 500 Hz octave band, source position – S1.

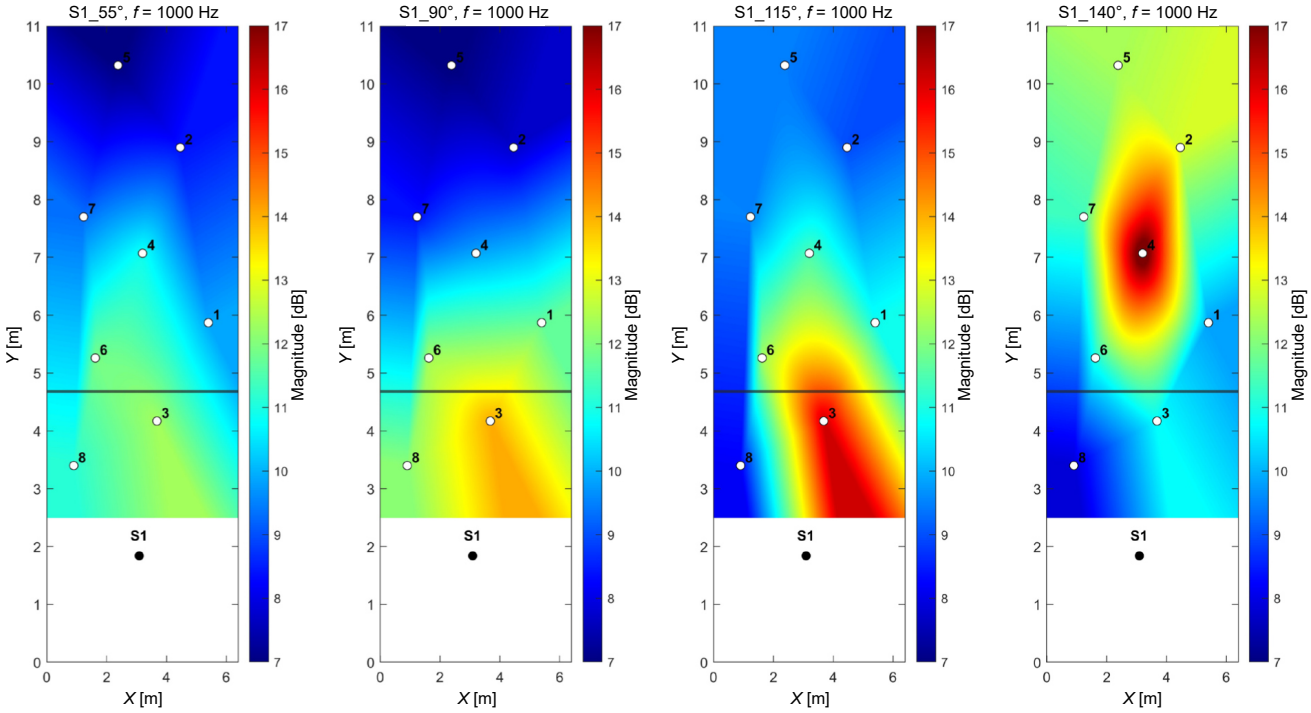

Fig. 10. SPL heatmaps for all PAL angles, 1 kHz octave band, source position – S1.

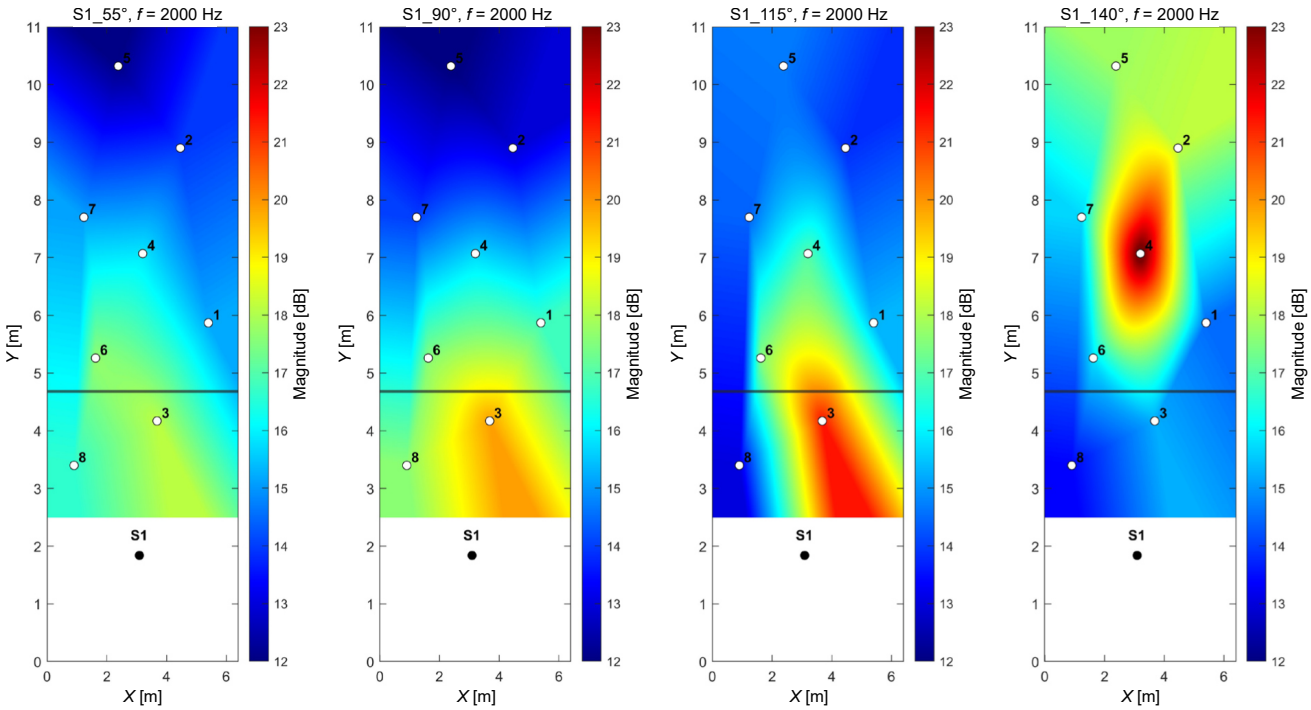

Fig. 11. SPL heatmaps for all PAL angles, 2 kHz octave band, source position – S1.

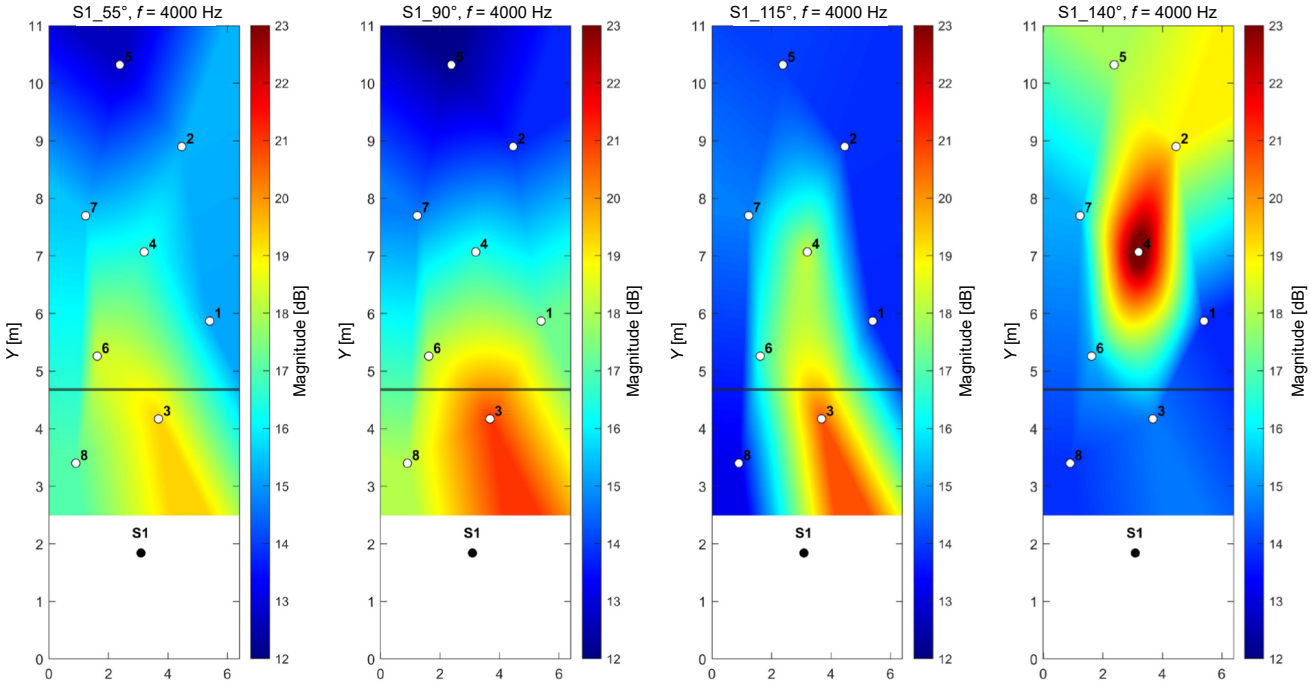

Fig. 12. SPL heatmaps for all PAL angles, 4 kHz octave band, source position – S1.

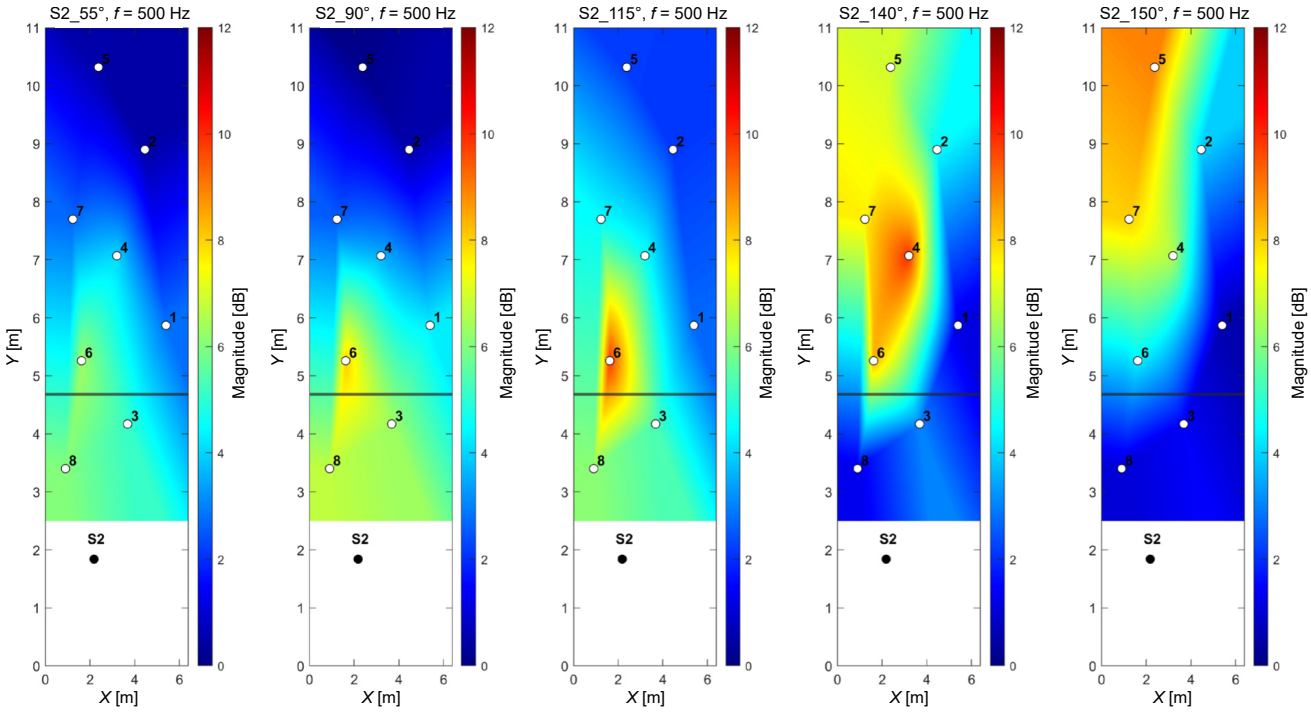

Fig. 13. SPL heatmaps for all PAL angles, 500 Hz octave band, source position – S2.

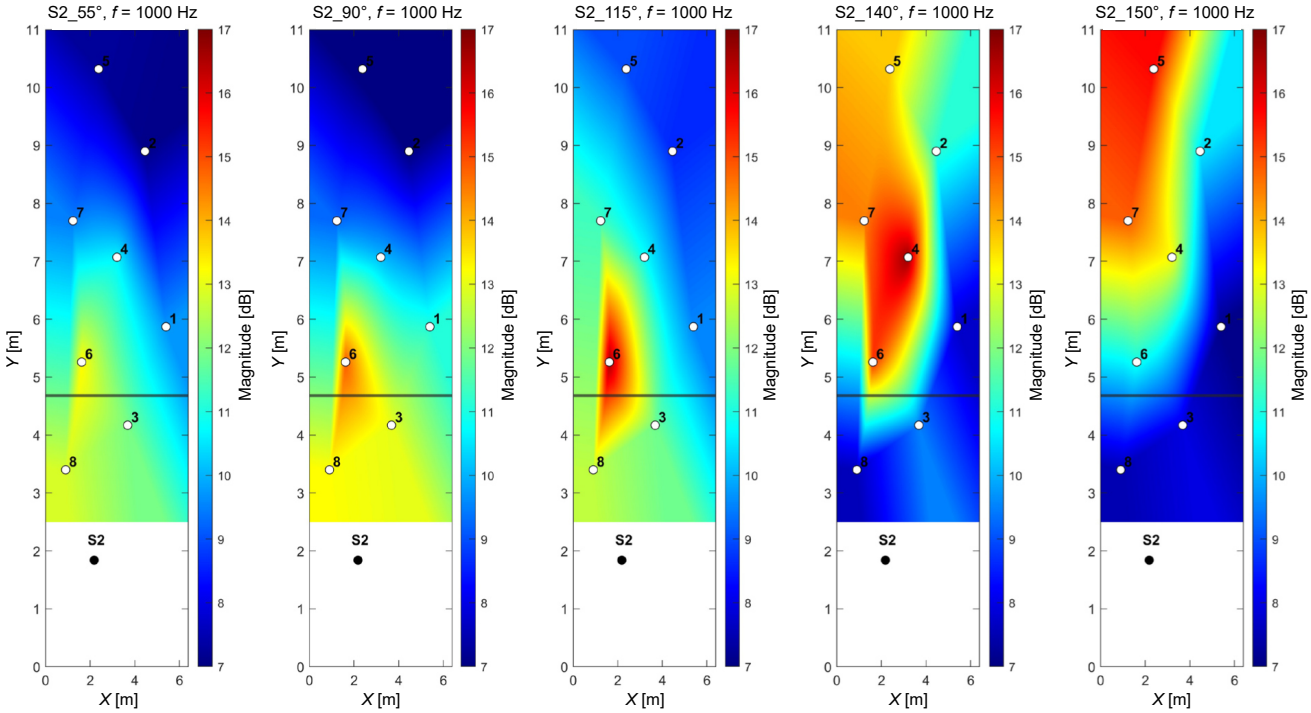

Fig. 14. SPL heatmaps for all PAL angles, 1 kHz octave band, source position – S2.

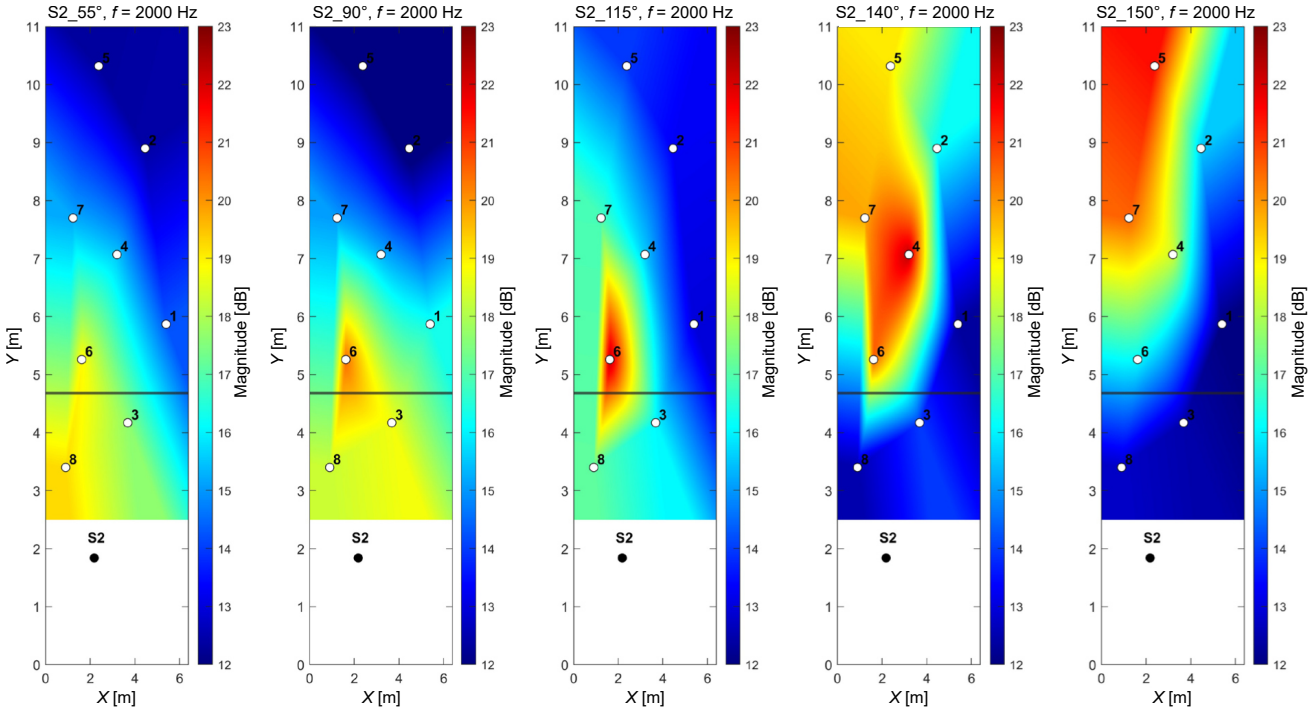

Fig. 15. SPL heatmaps for all PAL angles, 2 kHz octave band, source position – S2.

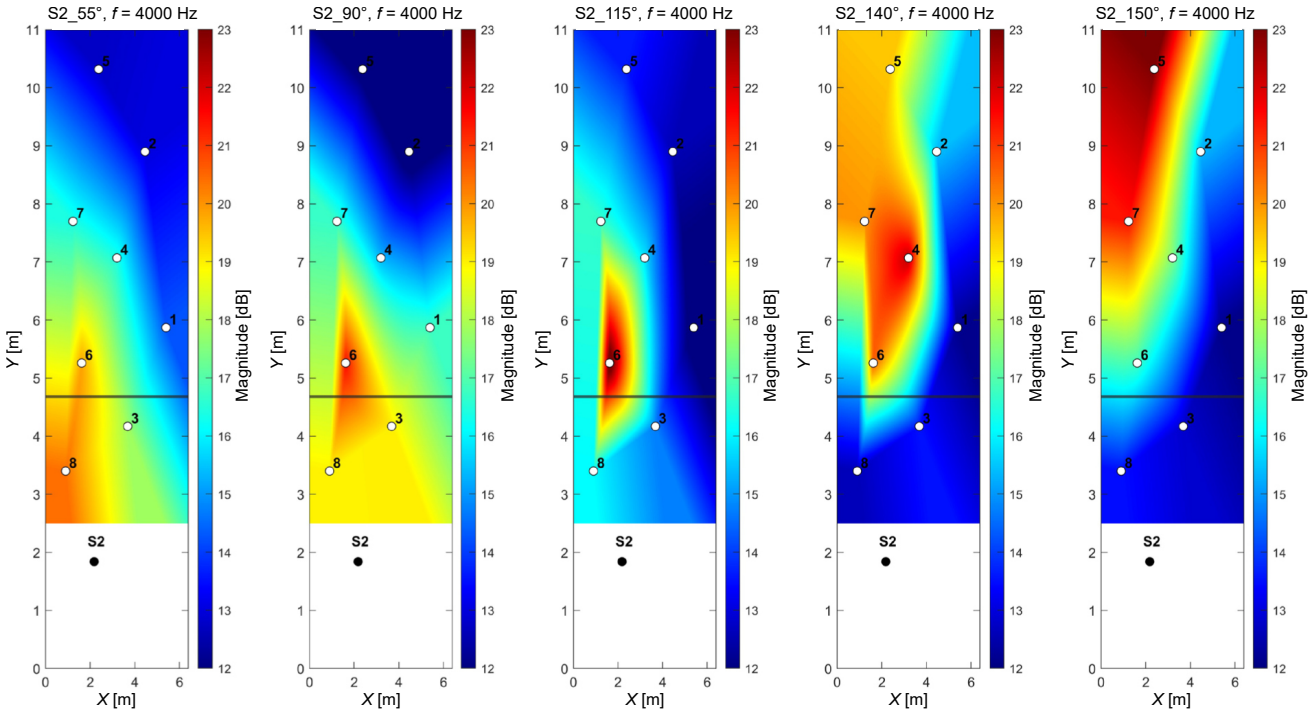

Fig. 16. SPL heatmaps for all PAL angles, 4 kHz octave band, source position – S2.

All of the presented maps show a strong concentration of sound at measurement points closest to the reflection path. Lower frequencies are more spread out than the higher frequencies, which proves that the presented method allows analysis of both geometric and wave phenomena, and that the obtained results match those acquired from laboratory experiments. Since the angle of 150° indicated that the PAL was pointed at the furthest edge of the angled ceiling, the values presented on the S2_150° heatmaps in Figs. 13–16 show the effective range of the said ceiling. High levels of sound pressure visible near the back wall of the room prove that its length is appropriate for the current room dimensions. As shown in the laboratory measurements, the area of a reflector needs to be large enough to reflect sound from lower frequency bands. Since the 500 Hz frequencies are visibly concentrated on the acquired maps, the size of the angled portion is also sufficient.

4.2. Simulation verification

To verify the results, the measured room was modelled and analysed in EASE Acoustic 4.4 using the raytracing module. The angled ceiling was included in the model, along with the measurement points. As shown in Fig. 17, reflections from the furthest edge of the angled portion of the ceiling are directed toward the last row of desks in the room. These results match those obtained from the in-situ measurements and confirm the effectiveness of parametric speakers in room acoustic analysis. Simulation outcomes for the S2 source were nearly identical to those acquired for S1; therefore, only the results for the S1 source are presented in this paper. It is important to emphasise that this method of analysis does not account for wave effects and was therefore used only to verify reflections at the incident angle. More advanced simulations will be carried out in future work.

4.3. Leave-one-out cross-validation of interpolation

To statistically verify the accuracy of the interpolation, the leave-one-out cross-validation (LOOCV) method was used, as it has the advantage of being applicable even with small samples (Geroldinger *et al.*, 2023). In this approach, a single observation is used for validation while the rest of the data forms the training dataset. This process is repeated so that each observation in the entire dataset is used only once for validation (Lumumba *et al.*, 2024). In this method, assume that we have the dataset D, where

$$D = \{(x_1, y_1)\,(x_2, y_2)\,, ..., (x_i, y_i)\}. \tag{2}$$

In this approach, x_i represents the features, in this case, the coordinates, and y_i represents the corresponding label of the outcome for each observation i (where $i = 1, 2, ..., n$), which in this case is the SPL for a given octave at one of the measurement points. Model training is conducted on $n-1$ observations and only one observation is used as the validation set, giving the classification error that can be expressed with the following mathematical equation (Lumumba *et al.*, 2024):

$$\text{LOOCV}_{\text{ERROR}} = \frac{1}{n}\sum_{i=1}^{n} L(y_i, \widehat{y}_i), \tag{3}$$

where L is the loss function and $\widehat{y}_i$ is the expected value for point i from a model trained without point i. The common loss function is the root mean squared error (RMSE), expressed as

$$L\,(y_i, \widehat{y}_i) = \sqrt{(y_i, \widehat{y}_i)}^{\,2}. \tag{4}$$

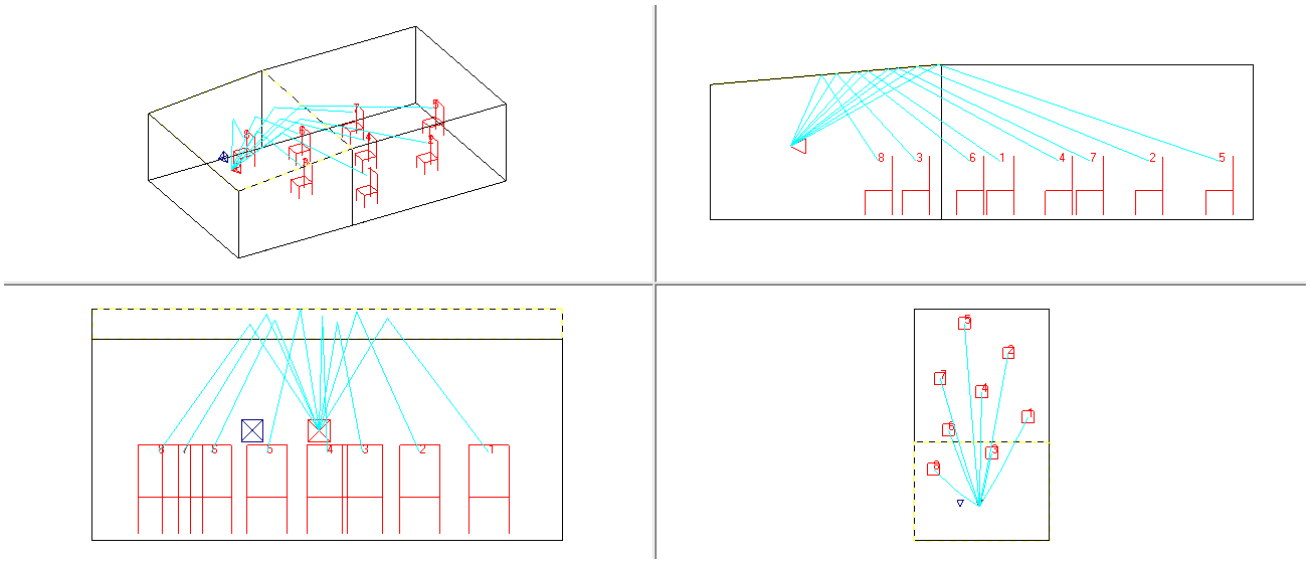

Fig. 17. Ray-tracing results of the measured room modelled in EASE Acoustic – S1 source.

This loss function is sensitive to large deviations, which makes it suitable for SPL measurements, as SPL varies significantly over short distances. The values of the loss function L calculated for all measurements are shown in Table 2.

Table 2. Loss function values calculated from LOOCV.

Source_angle	Loss function values in each bandwidth [dB]			
	500 Hz	1 kHz	2 kHz	4 kHz
S1_55°	1.2	1.2	1.5	2.0
S1_90°	1.1	1.1	1.2	1.5
S1_115°	2.9	3.1	3.4	3.6
S1_140°	2.7	2.8	3.0	3.4
S2_55°	1.0	1.0	1.0	1.1
S2_90°	1.4	1.5	1.8	2.1
S2_115°	2.1	2.2	2.8	3.8
S2_140°	3.5	3.7	3.9	3.9
S2_150°	2.1	2.2	2.3	2.5

As shown in Table 2, all loss function values are in the range of 1 dB–3.9 dB. This level of accuracy is not significant; however, since the differences between high and low sound pressure can vary drastically over short distances, even up to 10 dB, it is sufficient for this experiment. Since the measurements were preliminary, for further study, the density of the receiver grid should be increased to minimise the error.

5. Summary

This paper presented research results concerning the use of PALs in room acoustic analysis, especially for tracing reflection from highly reflective surfaces. In summary, it was found that certain models of PALs possess sufficiently narrow beamwidths to allow first-reflection analysis without interference from other elements in the room. The reflected sound exhibited a directivity pattern dependent on the panel size, with larger panels producing wider beamwidths and reflecting more energy at lower frequencies, which is consistent with wave phenomena typically observed in room acoustic measurements. Therefore, PALs can potentially be used interchangeably with omnidirectional speakers, without losing essential information about wave behaviour in a given sound field. The characteristics of the reflected sound were also found to be largely independent of the surface material, provided the material is sufficiently reflective. Consequently, panels made from different materials, such as wood or acrylic glass, should yield comparable results when measured with a PAL. Finally, it was demonstrated that PALs can be effectively utilised for assessing reflective elements in rooms and can reliably generate reflected sound distribution maps, allowing for precise evaluation of an element's acoustic performance.

Fundings

This research was funded by a research subvention supported by the Polish Ministry of Science and Higher Education (grant no. 16.16.130.942).

Conflict of interest

The authors declare that they have no known competing financial interests or personal relationships that could have appeared to influence the work reported in this paper.

Authors' contributions

Filip Węgrzyn conceptualized the study, wrote the original draft, conducted the measurements and performed the analysis. Adam Pilch conducted the measurements, contributed to data interpretation, edited the manuscript. All authors reviewed and approved the final manuscript.

References

1. Bennett M.B., Blackstock D.T. (1975), Parametric array in air, *Journal of the Acoustical Society of America*, **57**(3): 562–568, https://doi.org/10.1121/1.380484.
2. Berktay H.O. (1965), Possible exploitation of nonlinear acoustics in underwater transmitting applications, *Journal of Sound and Vibration*, **2**(4): 435–461, https://doi.org/10.1016/0022-460X(65)90122-7.
3. Gallien A., Prawda K., Schlecht S. (2024), Matching early reflections of simulated and measured RIRs by applying sound-source directivity filters, [in:] *Audio Engineering Society Conference: AES 2024 International Acoustics & Sound Reinforcement Conference*, https://aes2.org/publications/elibrary-page/?id=22373.
4. Gan W.-S., Yang J., Kamakura T. (2012a), Parametric acoustic array: Theory, advancement, and applications, *Applied Acoustics*, **73**(12): 1209–1210, https://doi.org/10.1016/j.apacoust.2012.06.016.
5. Gan W.-S., Yang J., Kamakura T. (2012b), A review of parametric acoustic array in air, *Applied Acoustics*, **73**(12): 1211–1219, https://doi.org/10.1016/j.apacoust.2012.04.001.
6. Geroldinger A., Lusa L., Nold M., Heinze G. (2023), Leave-one-out cross-validation, penalization, and differential bias of some prediction model performance measures – A simulation study, *Diagnostic and Prognostic Research*, **7**: 9, https://doi.org/10.1186/s41512-023-00146-0.
7. Ju H.S., Kim Y.-H. (2010), Near-field characteristics of the parametric loudspeaker using ultrasonic transducers, *Applied Acoustics*, **71**(9): 793–800, https://doi.org/10.1016/j.apacoust.2010.04.004.
8. Keele Jr. D.B. (2016), Design of free-standing constant beamwidth transducer (CBT) loudspeaker line arrays for sound reinforcement, *Journal of the Audio*

Engineering Society, https://aes2.org/publications/elibrary-page/?id=18428.

9. Login D. (2015), *A new approach to loudspeaker measurements*, Klippel GmbH, https://www.klippel.de/uploads/media/Logan_Klippel_Near_Field_Scanner_2015.pdf (access: 20.07.2025).
10. Lumumba V.W., Kiprotich D., Mpaine M.L., Makena N.G., Kavita M.D. (2024), Comparative analysis of cross-validation techniques: LOOCV, k-folds cross-validation, and repeated k-folds cross-validation in machine learning models, *American Journal of Theoretical and Applied Statistics*, **13**(5): 127–137, https://doi.org/10.11648/j.ajtas.20241305.13.
11. Rakerd B., Hunter E.J., Berardi M., Bottalico P. (2018), Assessing the acoustic characteristics of rooms: A tutorial with examples, *Perspectives of the ASHA Special Interest Groups*, **3**(19): 8–24, https://doi.org/10.1044/persp3.SIG19.8.
12. Tervo S., Pätynen J., Lokki T. (2009), Acoustic reflection path tracing using a highly directional loudspeaker, [in:] *2009 IEEE Workshop on Applications of Signal Processing to Audio and Acoustics*, pp. 245–248, https://doi.org/10.1109/ASPAA.2009.5346530.
13. Videotel Digital (2014), HyperSound® HSS 3000 mono/stereo system directional audio speakers, Turtle Beach Corporation, https://cdn.shopify.com/s/files/1/0260/5894/8671/files/HyperSound_Owners_Manual.pdf?v=1588116815 (access: 20.07.2025).
14. Vuine F. (2024), Loudspeaker, European Patent Office, Patent number EP4122215B1.
15. Westervelt P.J. (1963), Parametric acoustic array, *Journal of the Acoustical Society of America*, **35**(4): 535–537, https://doi.org/10.1121/1.1918525.
16. Yoneyama M., Fujimoto J.I., Kawamo Y., Sasabe Y. (1983), The audio spotlight: An application of nonlinear interaction of sound waves to a new type of loudspeaker design, *Journal of the Acoustical Society of America*, **73**(5): 1532–1536, https://doi.org/10.1121/1.389414.